Helv Phys Acta
Vol. 69 (1996)

0018-0238/96/010069-12$1.50+0.20/0

Photon escape cones in the Kerr field

By Oldřich Semerák

Department of Theoretical Physics, Faculty of Mathematics and Physics,
Charles University, V Holešovičkách 2, 180 00 Praha 8, Czech Republic

(13.III.1996)

Abstract. Solid angles spanning the directions along which photons can escape to infinity from a given point in the Kerr space are found with respect to the local stationary observers. The knowledge of the "photon escape cones" allows one to plot the outline of the Kerr source as seen by such observers. The results obtained are consistent with the expectation of the effects of frame dragging in rotating black hole geometries, whereas those for naked singularities are more complicated and less intuitive.

1 Introduction

One need not know relativity theory to take the statement "things may be different from how they appear" as trivial. However, relativity added a new dimension to this assertion, claiming (i) that we can learn about things only by means of signals propagating with velocities not greater than the velocity of light, and (ii) that we live in a curved spacetime, where signals do not travel along "straight lines". The former leads to aberration and Doppler effect, while the latter to the bending of rays, gravitational lensing in particular.

Predictions of the observational implications of relativistic effects on the propagation of light are crucial both for reconstructing the remote "reality" in astrophysics and for testing relativity itself. It is mainly owing to the growing number of sufficiently precise observational data and to the increasing computational facilities that such predictions are made in an ever growing number of articles, bringing the appearances, photometric curves, signal arrival times, spectra, line profiles and the polarization properties of radiation of sources (i) which are moving very fast with respect to the observer and/or (ii) whose light passes a strong

gravitational field somewhere on the way to him. (i) refers first to cosmic jets and their apparent superluminal motion, aberration and Doppler boosting, while (ii) [often in addition to (i)] refers to very compact objects (neutron stars, black holes, naked singularities) or to the sources orbiting around them (the single stars or the accretion discs with hot spots in particular) or lying far behind them (and sending light to be deflected or gravitationally lensed). The results summarized under "(ii)" are mostly based on computations of photon geodesics in a given gravitational background.

Since many highly active celestial sources appear to derive their power from processes involving very compact uncharged rotating bodies, it is the Kerr metric – describing the field of such bodies [1] – which is ascribed a particular astrophysical relevance. Most of the results on geodesic motion in the Kerr field were derived, reviewed, or at least cited, by [2–7]; the photon geodesics, in particular, were treated also e.g. by [8–10]. Here I notice explicitly the detail which in fact is involved in every scheme for visualization in the Kerr spacetime – numerical construction of the photon escape cones as seen by various stationary observers. The surfaces of these cones may be said, at least for black holes, to define the outlines of the Kerr source in the observer's viewing field. For previous considerations on this point see [11–13] (and cf. also e.g. [14, 15]).

There is hardly anything so efficient in providing an a priori intuition about the structure of spacetime as the graphic illustration of the light cones (in 4 dimensions) and of the photon escape cones (in 3 dimensions). Whereas the system of the light cones is being figured frequently, the sequence of the solid angles spanning the directions along which photons can escape to infinity is usually adduced only in the non-rotating, Schwarzschild case. General idea of how to obtain the photon escape cones for Kerr was given already in [11]. However, as the intuition about the Kerr field has entered into a wide awareness, there has been no urgent demand for adding the "missing details": escape cones has been expected simply to lean in the direction of the source's rotation, being dragged by the co-rotating gravitational field.

2 Specification of the problem

At each point of the Schwarzschild field the photon escape solid angles can be found analytically from the behaviour of the effective potentials. As seen by static observers, they are right circular (around radial lines going through the "starting" points); their vertex angle increases from 0° for $r \to r_{\rm g} = 2M$ via 180° at $r = r_{\rm ph} = 3M$ to 360° for $r \to \infty$. The Kerr geometry is *not* spherically symmetric and neither are the corresponding effective potentials, whence one cannot manage with the mere investigation of their courses without the exact knowledge at least of certain parts of the trajectories. Escape cones cannot be expected to be right circular, making the problem more complicated.

The Kerr spacetime, characterized by the mass M and the specific angular momentum

a, has the metric [1]

$$\mathrm{d}s^2 = -\frac{\Delta\Sigma}{\mathcal{A}}\,\mathrm{d}t^2 + \frac{\mathcal{A}}{\Sigma}\sin^2\theta\,(\mathrm{d}\phi - \omega_{\mathrm{K}}\mathrm{d}t)^2 + \frac{\Sigma}{\Delta}\,\mathrm{d}r^2 + \Sigma\mathrm{d}\theta^2\,, \tag{2.1}$$

where

$$\Delta = r^2 - 2Mr + a^2,\ \ \Sigma = r^2 + a^2\cos^2\theta,\ \ \mathcal{A} = (r^2+a^2)^2 - \Delta a^2\sin^2\theta,\ \ \omega_{\mathrm{K}} = 2Mar/\mathcal{A}, \tag{2.2}$$

and the Boyer-Lindquist coordinates $x^\mu = (t, r, \theta, \phi)$ and geometrized units ($c = G = 1$) are used. The radial motion of free test photons in this metric is described by the "radial" Carter equation [16] for massless particles,

$$\Sigma^2\dot{r}^2 = R(r) = P^2 - \Delta K = [(r^2+a^2)E - a\Phi]^2 - \Delta K. \tag{2.3}$$

The dot denotes differentiation with respect to the affine parameter normalized so that the photon's 4-momentum is $p^\mu = \dot{x}^\mu$. The photon's energy at infinity, E, the azimuthal component of its angular momentum at infinity, Φ, and the modified Carter's "fourth constant", $K(\geq 0)$, are constants of motion.

These can be expressed in terms of the components of photon's 4-momentum measured in some local tetrad at a given point, $p^{\hat{\alpha}}$. When using the stationary frame – the locally orthonormal frame tied to the observer orbiting uniformly in the ϕ-direction along constant r and θ, one obtains [17]

$$\Phi = \hat{E}u^t\sin\theta\,[(\mathcal{A}/\Sigma)\sin\theta\,(\omega - \omega_{\mathrm{K}}) + \sqrt{\Delta}\sin\hat{\alpha}\sin\hat{\beta}]\,, \tag{2.4}$$

$$E = \hat{E}/u^t + \omega\Phi\,, \tag{2.5}$$

$$K = P^2/\Delta - \Sigma\hat{E}^2\cos^2\hat{\alpha} = T^2 + \Sigma\hat{E}^2\sin^2\hat{\alpha}\cos^2\hat{\beta}\,, \tag{2.6}$$

where $T = aE\sin\theta - \Phi/\sin\theta$, $\omega = (\mathrm{d}\phi/\mathrm{d}t)_{\mathrm{SnO}}$ is the orbital angular velocity of the stationary observer relative to the rest frame at radial infinity, $u^\mu = u^t(1,0,0,\omega)$ is his 4-velocity, with $u^t = [1 - (2Mr/\Sigma)(1 - a\omega\sin^2\theta)^2 - (r^2+a^2)\omega^2\sin^2\theta]^{-1/2}$, $\hat{E}$ stands for the locally measured energy of the photon, and $\hat{\alpha}$ and $\hat{\beta}$ for the local latitudinal and azimuthal angles, i.e., for the locally measured deflection from the outward radial direction and orientation within the (θ,ϕ)-plane, respectively (see Fig. 1 in [7]).

Now the question goes like this: for some given a and initial point $(r_{\mathrm{in}}, \theta_{\mathrm{in}})$, what are the maximum values of $\hat{\alpha}_{\mathrm{in}}$, $\hat{\alpha}_{\mathrm{in}}^{\mathrm{max}}$ say, consistent with the photon's escape to radial infinity, for various $\hat{\beta}_{\mathrm{in}} \in \langle 0°, 360°)$? What are the dependences of $\hat{\alpha}_{\mathrm{in}}^{\mathrm{max}}$ on the parameters $a, r_{\mathrm{in}}, \theta_{\mathrm{in}}, \hat{\beta}_{\mathrm{in}}$?

3 Method of solution

The answers can be found numerically: for each single photon (specified by $r_{\mathrm{in}} > 0$, θ_{in}, $\hat{\alpha}_{\mathrm{in}}$, $\hat{\beta}_{\mathrm{in}}$) and a given a one computes the constants of motion (2.4)-(2.6) and takes the decision on its (in)capability of escape on the basis of the course of the function $R(r)$ on the right-hand side of eq. (2.3).

According to eq. (2.3), the motion of photons is only allowed in regions with $R(r) \geq 0$. The radius where R vanishes may either be a turning point – where the sense of the radial motion changes (this is the case when $R' = dR/dr \neq 0$ there), or the radius of a spherical orbit which the photon "winds up" on – where the radial motion ceases (this is the case when $R' = 0$ there). From the explicit form

$$R(r) = E^2 r^4 + [2aE(aE - \Phi) - K]r^2 + 2MKr + a^2[(aE - \Phi)^2 - K] \tag{3.1}$$

it is obvious that $R > 0$ for $r \to \pm\infty$, i.e., that far from the gravitational centre *any* photon can exist in principle. To be able to get there from a given location, it must not meet any root of R on the way.

These conditions, however, are not enough for photon which has not been launched outwards from the centre. If it starts in the direction *towards* the centre ($90° < \hat{\alpha}_{\rm in} \leq 180°$), there must, in addition, exist the root of R (with $R' > 0$) situated inside $r_{\rm in}$, which reflects the photon from the centre. This root must lie outside the outer horizon at

$$r = r_+ = M + (M^2 - a^2)^{1/2} \tag{3.2}$$

in the case of a black hole ($a \leq M$), while somewhere on the way to the asymptotic region of the negative-r sheet of the manifold in the case of a naked singularity ($a > M$);[1] If the photon is launched *tangentially* ($\hat{\alpha}_{\rm in} = 90°$), with $\dot{r}_{\rm in} = 0$, that is, just from the root of R, then R' must be positive there in addition.

Now, considering that

$$R(r_{\rm in}) \geq 0 \ \text{ and } \ R(r \to \pm\infty) > 0\,, \tag{3.3}$$

there must be a negative local minimum of the function R localized between the bounds of the prospective region of inaccessible radii above $r_{\rm in}$; on the other hand, the existence of inaccessible region below $r_{\rm in}$ (but reaching above r_+ if $a \leq M$) would imply the presence of a negative local minimum of R there (or the negativeness of R at r_+). So one can deduce the positions of roots from the positions and values of the local extremes and from the value of $R(r_+)$, thus reducing the classification of photons on the basis of solution of the quartic equation $R(r) = 0$ [see (3.1)] to the problem requiring the solution of just a cubic equation, $R'(r) = 0$ – explicitly

$$r^3 + [a(a - \Phi/E) - K/(2E^2)]r + MK/(2E^2) = 0\,. \tag{3.4}$$

Checking also the positions of the inflection points from the equation $R''(r) = 0$ – explicitly

$$3r^2 + a(a - \Phi/E) - K/(2E^2) = 0 \ - \tag{3.5}$$

– and possibly regarding that

$$R(r; K = 0) = P^2 \geq 0, \ \ R(r = r_+) = P^2(r_+) \geq 0, \ \ R'(r = 0) = 2MK \geq 0, \tag{3.6}$$

one has enough information about the course of $R(r)$ to learn (i) whether there is no obstacle in the photon's way to radial infinity and, for $\hat{\alpha}_{\rm in} > 90°$, also (ii) whether there is something to reflect it away from the centre.

[1] For the global structure of the Kerr spacetime see e.g. [18].

4 Numerical results

I present several typical outcomes to the numerical treatment of the problem. Figs. 1-3 show the dependence of $\hat{\alpha}_{\rm in}^{\rm max}$ on $\hat{\beta}_{\rm in}$ at several radii $r_{\rm in} \leq 20M$ in the equatorial plane of the Kerr fields with $a = 0$, M and $1.3M$. Mostly the radii

$$r_{\rm in}^{(j)} = B \cdot 10^{\log(20/R)(j/10)^k} \quad (j = 1, 2, ..., 10) \tag{4.1}$$

were chosen (just for graphical reasons), with $B = r_+$ and $k = 2$ for $a \leq M$, and with $B = 0.04M$ and $k = 1$ for $a > M$ (see Figure captions for concrete values); that static frames may actually exist only above the static limit, and the freely orbiting frames above the corresponding circular photon geodesics and at nowhere other than $\theta = 90°$, is, of course, respected. Figs. 1-3 are presented in the form of polar diagrams, where the increase of $\hat{\alpha}_{\rm in}$ from 0° to 180° appears as a shift from their centre to the periphery, $\hat{\beta}_{\rm in}$ going round about. Figs. 4 show the dependences of $\hat{\alpha}_{\rm in}^{\rm max}$ on $r_{\rm in}$ for $\hat{\beta}_{\rm in} = 90°$, 180° (or 0°) and 270°, at $\theta_{\rm in} = 0°$, 15°, 30°, ..., 90°, in the extreme Kerr ($a = M$). The courses of $\hat{\alpha}_{\rm in}^{\rm max}(r_{\rm in})$ along the symmetry axes of backgrounds with $a/M = 0.0$, 0.2, 0.4, ..., 1.0, 1.01, 1.1, 1.2, 1.4, 1.6, ..., 5.0 are depicted in Fig. 5.

In the Figure captions I use the abbreviations LNRF, CF, SF and FOF±, respectively for the particular, privileged cases of stationary frames (see [17]) – the locally non-rotating frame, the Carter frame, the static frame and the one tied to the observer on co/counter -rotating equatorial circular geodesic. In Figs. 4 and 5, the values of $r_{\rm in}$ are given (along the horizontal axis) in units of M.

From Figs. 1-3 (and also 5) it is evident that there are differences in shapes of the escape cones between the black-hole and the naked-singularity cases. For $a \leq M$, the results essentially confirm what one expects to find, namely (i) that the geometry around a spinning body tips the escape cones in the direction of its rotation and this effect strengthens with increasing a; (ii) that with $r_{\rm in}$ getting larger, photons escape more easily and also the influence of the centre's rotation weakens; (iii) that the "dragging of the escape cones" is stronger in the equatorial regions than close to the rotation axis; (iv) that photons escape more easily in prograde ($\hat{\beta}_{\rm in} = 90°$) than in retrograde ($\hat{\beta}_{\rm in} = 270°$) directions.

The rotating geometry drags the escape cones very effectively. They are almost tipped over to the $(+\phi)$-direction close to the extreme black hole (Figs. 2, 4); the prograde direction is so "advantageous" there that $\hat{\alpha}_{\rm in}^{\rm max}(\hat{\beta}_{\rm in} = 90°)$ often no longer goes to 0° when the starting point approaches the event horizon from outside (Figs. 4). The photons' ability to escape in a direction perpendicular to the rotation of the geometry ($\hat{\beta}_{\rm in} = 0°, 180°$) is, for fixed $r_{\rm in}$, almost independent of $\theta_{\rm in}$ and $\hat{\alpha}_{\rm in}^{\rm max}(\hat{\beta}_{\rm in} = 0°) = \hat{\alpha}_{\rm in}^{\rm max}(\hat{\beta}_{\rm in} = 180°)$, the latter resulting from the fact that $\hat{\beta}_{\rm in}$ enters the constants of motion merely in $\sin\hat{\beta}_{\rm in}$ [see (2.4)] and $\cos^2\hat{\beta}_{\rm in}$ [see (2.6)]. On the other hand, $\hat{\alpha}_{\rm in}^{\rm max}(\hat{\beta}_{\rm in} = 90°)$ increases and $\hat{\alpha}_{\rm in}^{\rm max}(\hat{\beta}_{\rm in} = 270°)$ decreases with $\theta_{\rm in}$ going from the axis towards the equatorial plane.

Figure 1 (below): The dependence of $\hat{\alpha}_{\rm in}^{\rm max}$ on $\hat{\beta}_{\rm in}$ in the Schwarzschild field ($a = 0$), at the radii [by (4.1)] $r_{\rm in}/M = 2.047, 2.193, 2.461, 2.891, 3.557, 4.582, 6.181, 8.730, 12.913, 20.000$.
a) ... with respect to the static frame (which is the limit of both the Kerrian LNRF, CF and SF).
b) ... with respect to the FOF. In comparison with a), the inner 4 cones are missing, their initial radii lying below the limiting photon orbit at $r_{\rm ph}(a = 0) = 3M$; on the other hand, two extra (the innermost ones) are added – at $r_{\rm in} = 3.001M$ and $3.1M$. The cones gradually "peel off" the value $\hat{\alpha}_{\rm in}^{\rm max} = 90°$. □

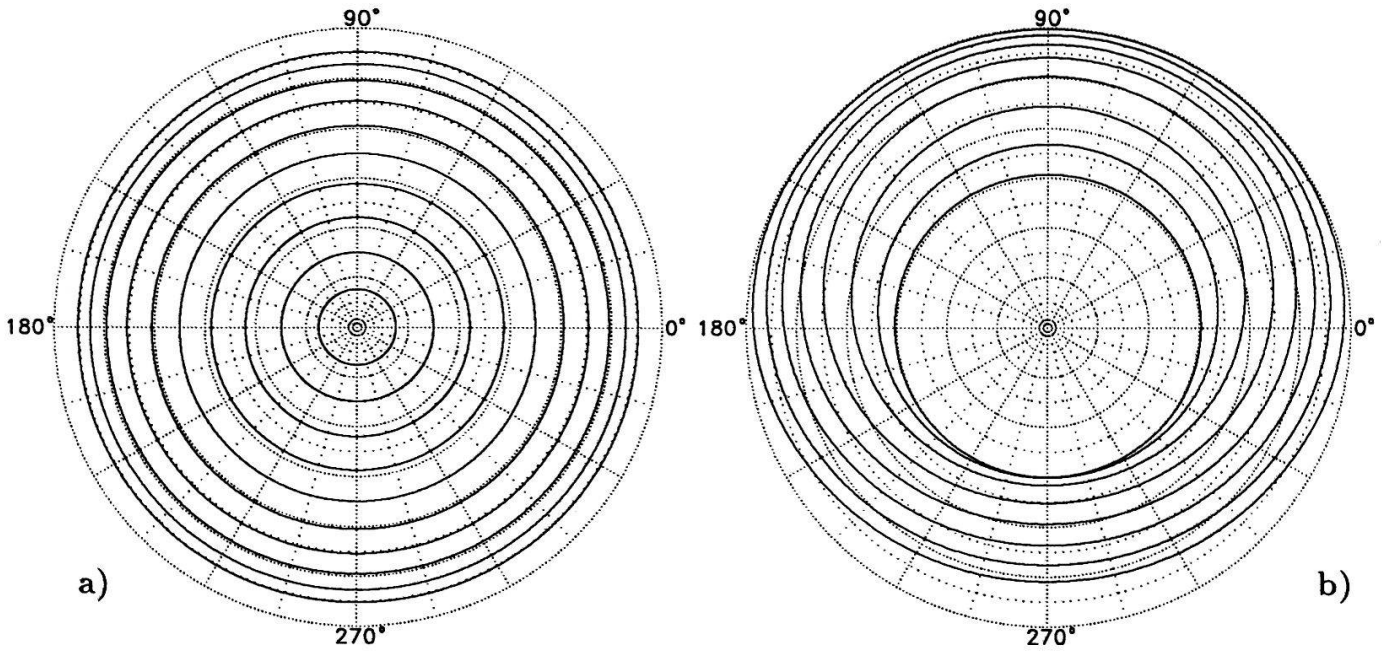

Figure 2 (on next page): The dependence of $\hat{\alpha}_{\rm in}^{\rm max}$ on $\hat{\beta}_{\rm in}$ in the equatorial plane ($\theta = 90°$) of the extreme Kerr field ($a = M$), at the radii [by (4.1)] $r_{\rm in}/M = 1.030, 1.127, 1.309, 1.615, 2.115, 2.940, 4.340, 6.802, 11.320, 20.000$. In Figs. a-c) and e) the escape cones widen gradually with increasing $r_{\rm in}$. In Fig. d) the contours demarcate, on the contrary, the *non*-escape sectors – by which photons fall to the hole (they narrow gradually with increasing $r_{\rm in}$).
a,b) ... with respect to the LNRF and CF, respectively.
c) ... with respect to the SF. In comparison with a,b), the inner 4 cones are missing, their initial radii lying below the outer static limit at $r_0(\theta = 90°) = 2M$; on the other hand, two extra cones (the first and the third from the centre) are added – at $r_{\rm in} = 2.01M$ and $2.35M$.
d) ... with respect to the FOF+. Here all 10 cones are given as in a,b) (namely the limiting co-rotating circular photon orbit is at $r_{\rm ph+}(a = M) = M$).
e) ... with respect to the FOF−. In comparison with a,b), the inner 6 cones are missing, their initial radii lying below the counter-rotating circular photon orbit at $r_{\rm ph-}(a = M) = 4M$; on the other hand, two extra (the first and the third from the centre) are added – at $r_{\rm in} = 4.001M$ and $5.1M$. The cones gradually "peel off" the value $\hat{\alpha}_{\rm in}^{\rm max} = 90°$. □

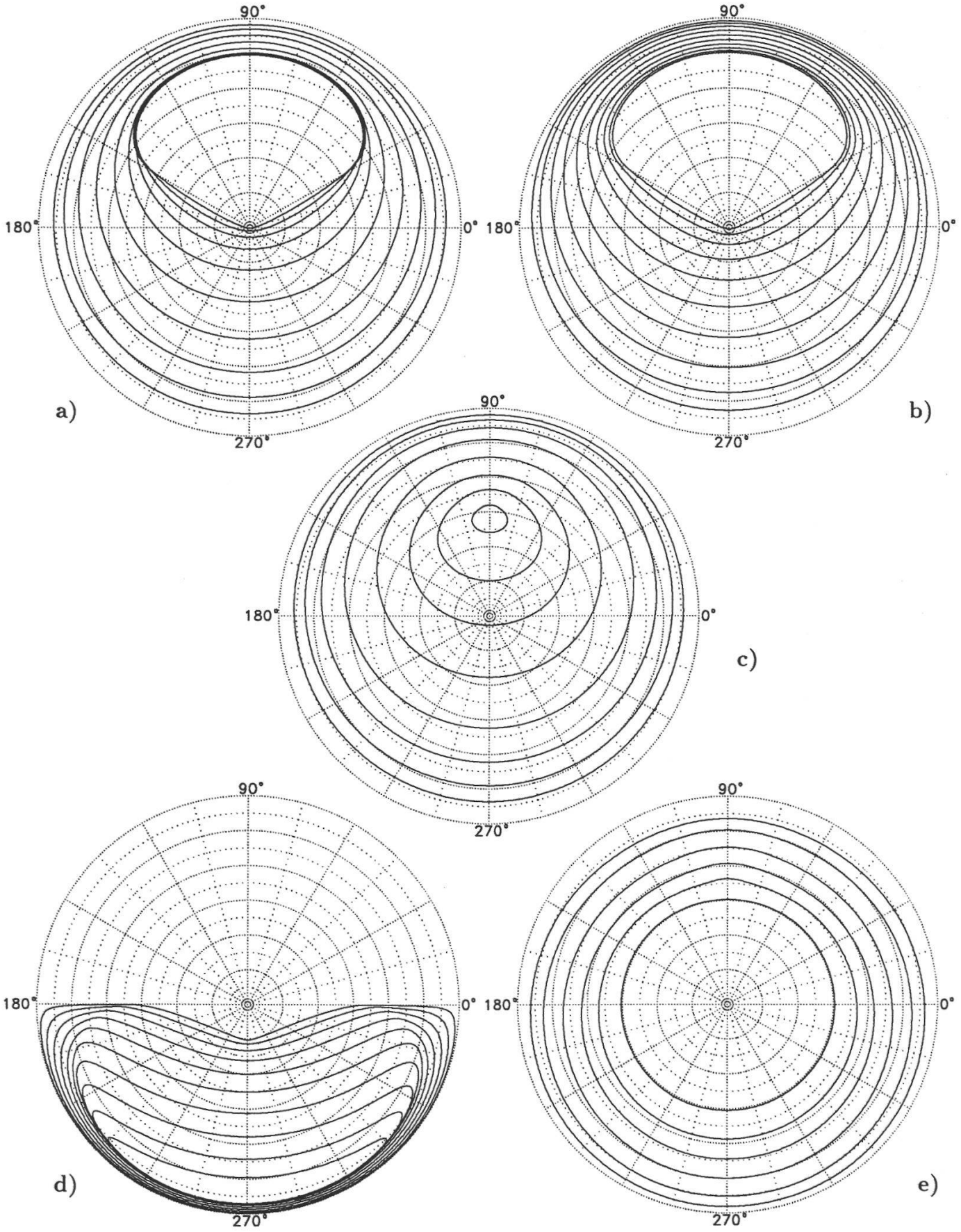
90°
180°
0°
270°
a)
b)
c)
d)
e)

Figure 3 (below): The dependence of $\hat{\alpha}_{\rm in}^{\rm max}$ on $\hat{\beta}_{\rm in}$ at $\theta = 90°$ for $a = 1.3M$.
a) ... with respect to the LNRF. The *non*-escape sectors are indicated at $r_{\rm in}/M = 0.074$, 0.139, 0.258, 0.480, 0.894, 1.665, 3.100, 4.200. They narrow with increasing $r_{\rm in}$ and finally disappear with $r_{\rm in}$ slightly greater than $4.2M$.
b) ... with respect to the CF. The *non*-escape sectors at $r_{\rm in}/M = 0.015$, 0.180, 0.480, 0.894, 1.665, 3.100, 4.200. With increasing $r_{\rm in}$ they first grow as ovals, then, elongating gradually to a banana shape, shrink and disappear with $r_{\rm in}$ slightly greater than $4.2M$.
c) ... with respect to the SF. In the upper part, the escape cones widen gradually at $r_{\rm in}/M = 2.01$, 2.08, 2.20 and 2.34; then they "switch over" to "*non*-escape cones" and narrow at $r_{\rm in}/M = 2.35$, 2.60, 3.10, 3.70 and 4.20 in the lower part.
d) ... with respect to the FOF+. The *non*-escape sectors are shown at $r_{\rm in}/M = 0.0001$, 0.025, 0.180, 0.894, 1.665, 3.100, 4.200. Their behaviour resembles that found in b).
[Fig. e) is not given, since here *all* of the photons launched by the FOF− can escape.] □

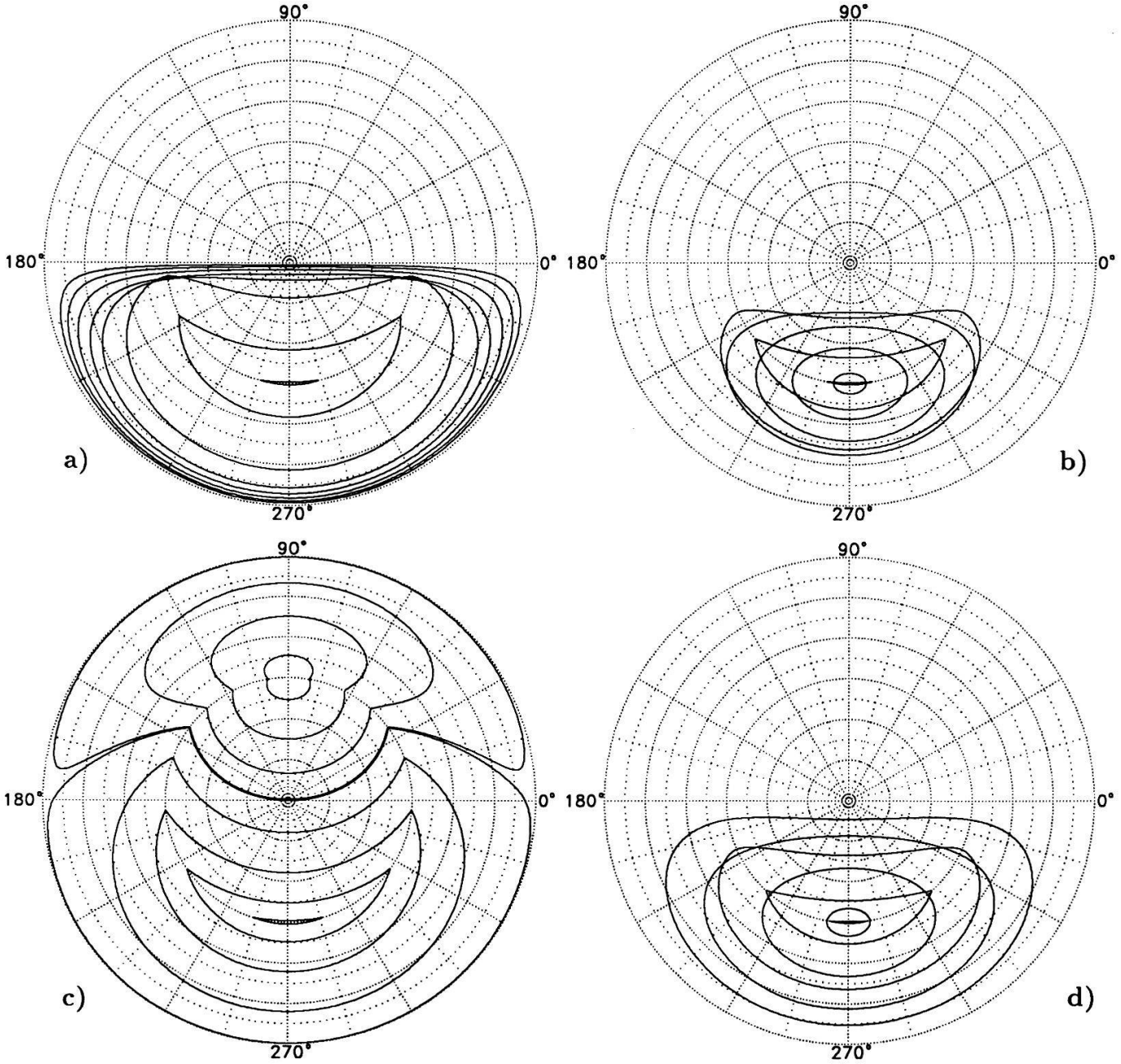

Figure 4: The radial course of $\hat{\alpha}_{\rm in}^{\rm max}$ at $\theta_{\rm in} = 0°, 15°, 30°, \ldots, 90°$ of the extreme Kerr field ($a = M$), for $\hat{\beta}_{\rm in} = 90°$ (dotted lines), $180°/0°$ (full lines) and $270°$ (dashed lines).
a,b) ... with respect to the LNRF, CF. With increasing $\theta_{\rm in}$, dotted lines shift up, dashed lines down, and full lines very slightly up.
c) ... with respect to the SF (and thus beginning only from the static limit). Here the full lines shift slightly down at $r_{\rm in} < 12.5M$ and slightly up at $r_{\rm in} > 12.5M$.
d,e) ... with respect to the FOF+/− (thus only at $\theta_{\rm in} = 90°$ and beginning only from the photon orbits). In d), the directions $\hat{\beta}_{\rm in} = 90°$ and $180°/0°$ are escape for *any* $\hat{\alpha}_{\rm in}$. □

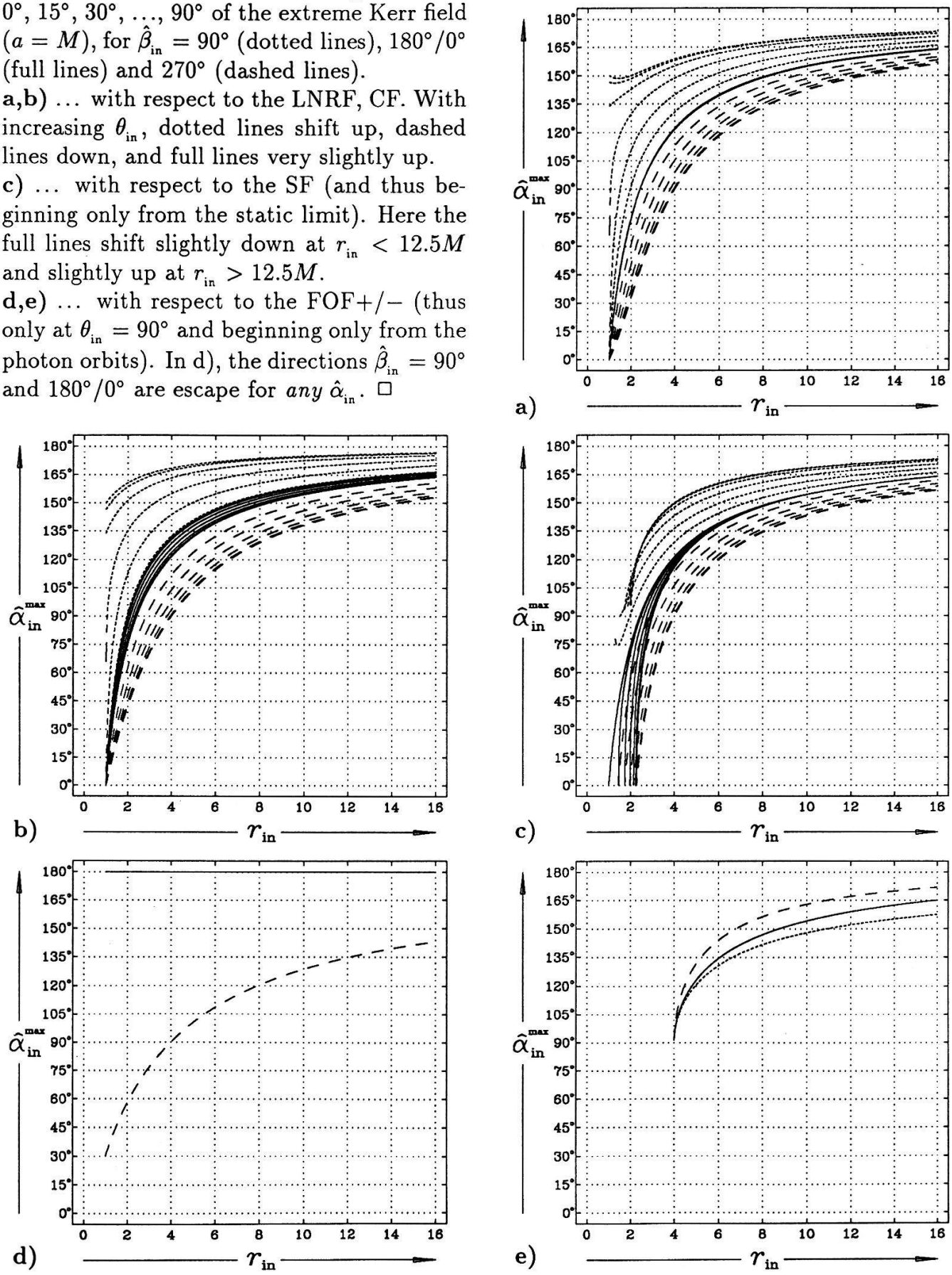

Figure 5 (below): The radial courses of $\hat{\alpha}_{\rm in}^{\rm max}$ on the symmetry axis of backgrounds with a/M = 0.0, 0.2, 0.4, ..., 1.0, 1.01, 1.1, 1.2, 1.4, 1.6, ..., 4.4. With increasing a, the lines shift gradually up for $a \leq M$, whereas (as taken at $r > 0$) down for $a > M$. Notice that for $a > M$ the lines intersect 90° only below $r_{\rm in} = 0$. This is due to the "repulsive" nature of the field inside the spheroidal domain spanned by the ring singularity: the trajectories are being "expelled" from the region just behind $r = 0$. (For still greater a the curves flatten further towards 90°.) □

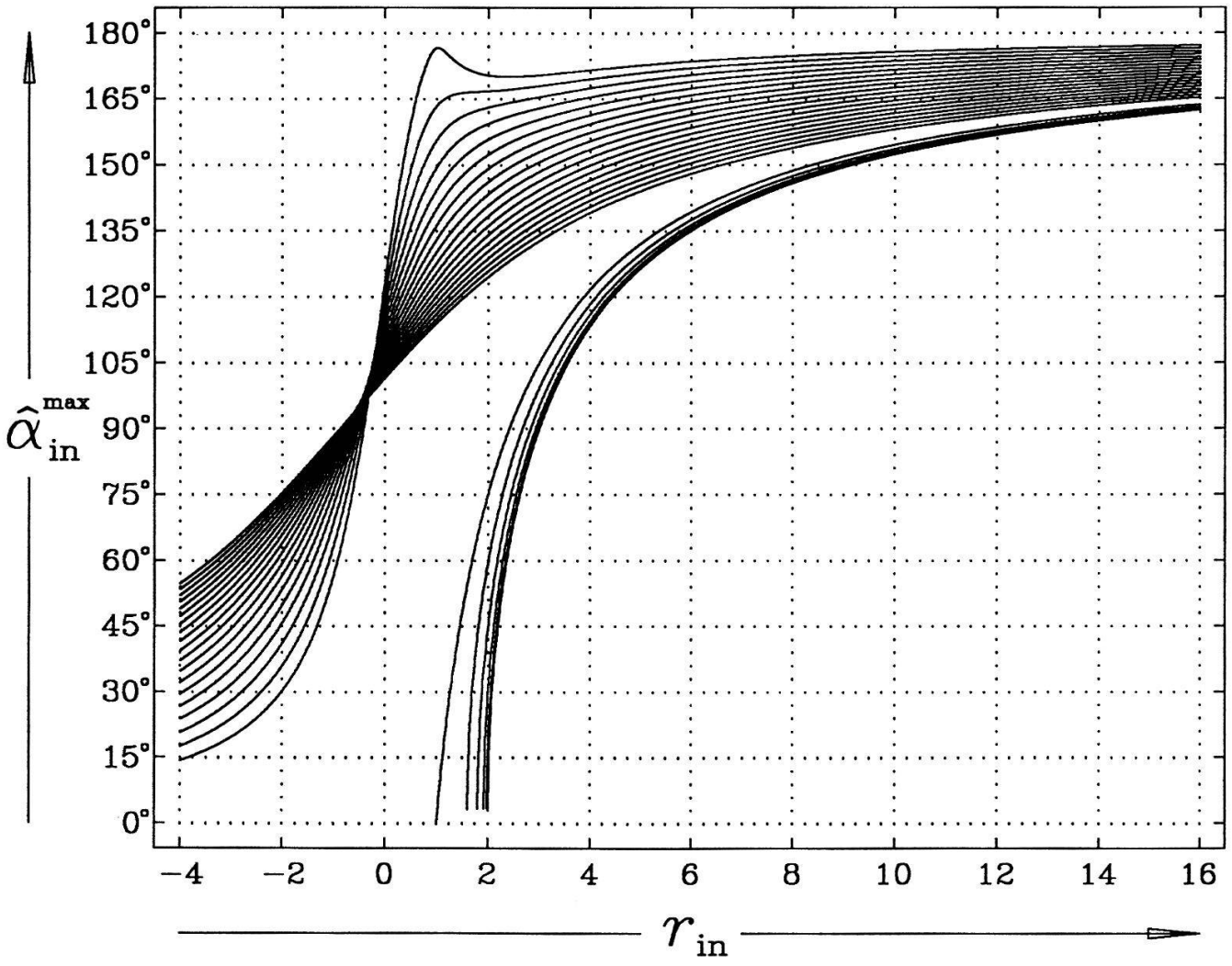

The curves one obtains for $a > M$ often differ from their black-hole counterparts considerably. In general, the dependences of $\hat{\alpha}_{\rm in}^{\rm max}$ on $r_{\rm in}$, $\theta_{\rm in}$ and, in particular, on $\hat{\beta}_{\rm in}$ (the shapes of the escape cones' surfaces), are quite complicated. Some of their features may be apprehended simply by realizing the ring shape of the naked singularity which, as opposed to the spheroidal shape of a black hole horizon, makes (loosely speaking) different the very geometrical meaning of different values of $\hat{\beta}_{\rm in}$. In particular, a small change in $\hat{\beta}_{\rm in}$ may shift the initial direction from outside the singular ring ($r = 0$, $\theta = 90°$) to inside it, thus altering drastically the character of the resulting photon trajectory. Anyway, in the naked space-

time there are more types of photon trajectories: the photons, in principle, can escape to $r \to +\infty$, to $r \to -\infty$, remain bound between two regions of forbidden radii, and some of those tied down to the equatorial plane may also hit the singularity; around the black holes, on the other hand, there are just photons escaping to infinity and those (to be) swallowed by the centre – with the exception of the (unstable) spherical polar and circular equatorial orbits, there are no spatially bound photon orbits of infinite length, which would oscillate between two radii above the horizon.

No escape cones constructed at $0° < \theta_{\rm in} < 90°$ in the naked spacetimes are shown, because the results are in general rather complicated there, consisting of *two* disjoint non-escape sectors within the escape zone. These dwindle with increasing $r_{\rm in}$ – one in a manner like in Fig. 3 and the other in the upper half of the diagram. In any case, one is lead again to a positive answer to the query [5] as to whether there are any essential differences between the manifestations of spacetimes with naked singularities and those with singularities concealed behind event horizons (cf. [7, 19]).

Acknowledgements

I thank Prof. Jiří Bičák for suggesting the problem and discussions, Dr. Petr Hadrava for help with figures, and Dr. Chris Chambers for critical reading of the typescript and suggesting a number of improvements. The work has been partly supported by the grant GACR-202/96/0206 of the Grant Agency of the C.R. and by the grant GAUK-318 of the Charles University.

References

[1] C.W. Misner, K.S. Thorne and J.A. Wheeler, *Gravitation* (Freeman 1973), Chapt. 33

[2] J. Stewart and M. Walker, Springer Tracts Mod. Phys. *69*, 69 (1973)

[3] O.P. Krivenko, K.A. Pyragas and I.T. Zhuk, Astrophys. Space Sci. *40*, 39 (1976)

[4] N.A. Sharp, Gen. Rel. Grav. *10*, 659 (1979)

[5] S. Chandrasekhar, *The Mathematical Theory of Black Holes* (Oxford Univ. Press 1983), Chapt. 7

[6] I.G. Dymnikova, Sov. Phys. Usp. *29*, 215 (1986)

[7] J. Bičák, O. Semerák and P. Hadrava, Mon. Not. R. Astron. Soc. *263*, 545 (1993)

[8] R.M. Floyd and B.A.V. Sheppee, Int. J. Theor. Phys. *6*, 281 (1972)

[9] T.M. Helliwell and A.J. Mallinckrodt, Phys. Rev. D *12*, 2993 (1975)

[10] Z. Stuchlík, Bull. Astron. Inst. Czechosl. *32*, 40 (1981)

[11] J.M. Bardeen, in *Black Holes*, ed. C. DeWitt and B.S. DeWitt (Gordon and Breach 1973), p. 215

[12] S.L. Shapiro, Astrophys. J. *189*, 343 (1974)

[13] M. Colpi, L. Maraschi and A. Treves, Astrophys. J. *311*, 150 (1986)

[14] S. Pineault and R.C. Roeder, Astrophys. J. *212*, 541, and *213*, 548 (1977)

[15] S.U. Viergutz, Astron. Astrophys. *272*, 355 (1993)

[16] B. Carter, Phys. Rev. *174*, 1559 (1968)

[17] O. Semerák, Gen. Rel. Grav. *25*, 1041 (1993)

[18] S.W. Hawking and G.F.R. Ellis, *The Large Scale Structure of Space-Time*, (Cambridge Univ. Press 1973), Chapt. 5.6

[19] O. Semerák, Czech. J. Phys. *45*, 1 (1995)